Published Version: **DOI**: 10.1016/j.chemolab.2018.12.007.

Investigating Native State Fluorescence Emission of Immunoglobulin G using polarized Excitation Emission Matrix (pEEM) spectroscopy and PARAFAC.

Marina Steiner-Browne, Saioa Elcoroaristizabal, Yannick Casamayou-Boucau, and Alan G. Ryder*
Nanoscale BioPhotonics Laboratory, School of Chemistry, National University of Ireland, Galway, Galway, H91CF50, Ireland.

Tel: 353-91-492943 **Email:** alan.ryder@nuigalway.ie

Citation: Investigating Native State Fluorescence Emission of Immunoglobulin G using polarized Excitation Emission Matrix (pEEM) spectroscopy and PARAFAC. M. Steiner-Browne, S. Elcoroaristizabal, Y. Casamayou-Boucau, and A.G. Ryder. *Chemometrics and Intelligent Laboratory Systems*, 185, 1-11 (**2019**).

DOI: 10.1016/j.chemolab.2018.12.007.

Abstract

Intrinsic fluorescence spectroscopy (IFS) measurements for protein structural analysis can be enhanced by the use of anisotropy resolved multidimensional emission spectroscopy (ARMES). ARMES attempts to overcome the tryptophan (Trp) and tyrosine (Tyr) spectral overlap problem and resolve emitting components by combining anisotropy measurements with chemometric analysis. Here we investigate for the first time the application of polarized excitation-emission matrix (pEEM) measurements and Parallel Factor (PARAFAC) analysis to study IFS from an Immunoglobulin G (IgG) type protein, rabbit IgG (rIgG), in its native state. Protein IFS is a non-trilinear system primarily because of Förster resonance energy transfer (FRET). Non-trilinearity is also caused by inner filter effects, and Rayleigh/Raman scattering, both of which can be corrected by data pre-processing. However, IFS FRET cannot be corrected for, and thus here we carefully evaluated the impact of various different data pre-processing methods on IFS data which used for PARAFAC. Care must be taken with data pre-processing and interpolation, as both had an impact on PARAFAC modelling and the recovered anisotropy values, with residual shot noise from the Rayleigh scatter which overlapped the emission blue edge being the root cause.

pEEM spectra from thawed rIgG solutions (15–35 °C temperature range) were collected with an expectation being that this temperature range should cause sufficient emission variation to facilitate component resolution but without major structural changes. However, the only significant changes observed were of the overall intensity due to thermal motion induced quenching and this was confirmed by the PARAFAC scores. PARAFAC resolved one major component (>99%) for the emission data (polarized and unpolarized) which mostly represented the large Tyr-to-Trp hetero-FRET process, with a second, very weak component (<1%) apparently a contribution from directly excited Trp emission. PARAFAC scores recovered from normalized pEEM data showed minimal change which was further proof for negligible structural change. The results of this study serves as the starting point for the use of PARAFAC analysis of IFS from IgG type proteins and important processes such as denaturation and aggregation.

Published Version: **DOI**: 10.1016/j.chemolab.2018.12.007.

Keywords: Protein, Immunoglobulin G, Fluorescence, Multidimensional, Spectroscopy, Anisotropy, PARAFAC.

1 Introduction

Immunoglobulin G (IgG) is a common class of antibody which is often used for therapeutic purposes [1, 2]. Monoclonal antibodies (mAb) have become a very significant class of active pharmaceutical ingredients (API) because of their high specificity, and the leveraging of the immense resources applied to studying the human genome. IgG type proteins in general have a flexible 'Y'-shaped structure, composed of two regions: a constant (Fc), and a variable region (Fab), connected by di-sulphide bonds and a hinge region (~150 kDa). Changes in the Fab portion amino acid sequence are responsible for IgG diversity (Figure S1, SI) while variations in the connection between Fab and Fc portion produces different IgG isotypes, which are species dependent. Humans have four isotypes [3, 4], while rabbits have only one [5-7]. These Fab portion differences between IgG isotypes, as well as changes in amino acid sequences, and protein structure regulate protein stability which is an important consideration for their use as APIs [8, 9].

Protein structure changes with physical and chemical stresses and the most serious involves tertiary structure unfolding which can lead to refolding into new structures and/or aggregation. These changes can cause a loss in function and potentially adverse immunogenicity issues [10]. Stresses can be induced by improper manipulation during manufacturing, storage or use and thus understanding and measuring the stability of proteins in solution is therefore, a key factor in ensuring efficacy and safety. The various quality attributes of therapeutic proteins can be monitored and measured using a variety of techniques. For example, high-performance liquid chromatography-size exclusion (HPLC-SEC) and dynamic light scattering (DLS) are most commonly used to assess protein aggregation [11]. Spectroscopic methods, such as circular dichroism (CD) and Fourier transform infrared (FTIR) can also be used to characterize the native structure and monitor changes in protein structure [12, 13]. While far-UV CD is sensitive to changes in secondary structure, near-UV CD detects changes in tertiary structure, protein concentration has to be carefully selected, as sedimentation and light scattering can negatively impact CD. FTIR can be used with liquid and solid samples in high concentrations and with large aggregates, but proteins can bind/adhere to the crystal and the water signal has to be carefully removed from the spectra. Therefore, a combination of different analytical tools, some of which are expensive and time consuming, are required to characterize protein structure and stability in solution [14].

Intrinsic fluorescence spectroscopy (IFS), which is non-destructive, can also be used to study protein structure in solution, due to the presence of phenylalanine (Phe), tyrosine (Tyr), and tryptophan (Trp) fluorophores in proteins [15]. Protein emission is mostly comprised of overlapping emission from Tyr and Trp because Phe has a very low quantum yield [15, 16]. Förster resonance energy transfer (FRET) is critical in IFS and determines how much emission from each fluorophore can be detected. For example, Phe with its small quantum yield, also undergoes FRET to Tyr or Trp [15], thus, Phe fluorescence cannot usually be discriminated in the presence of the much stronger Tyr or Trp emission. Similarly, the strong spectral overlap between Tyr emission and Trp absorbance also leads to high FRET rates; therefore, protein emission is dominated by Trp if present. In IgG type proteins with multiple Trp (~20/30) and Tyr (~50/60) present (Figure S1, SI), many located within a Förster radius of

each other, the rates of homo- and hetero-FRET will be high, leading to Trp dominated emission. At longer excitation wavelengths, λ_{ex}≥295 nm, Trp is preferentially excited and there is minimal Tyr excitation, therefore it is common to use λ_{ex}=295 nm for monitoring tertiary structural changes in proteins caused by physical or chemical stresses [11, 17, 18].

For the analysis of multi-fluorophore proteins or mixtures, multidimensional fluorescence spectroscopy (MDF) provides more information. The most common measurement methods are excitation-emission matrix (EEM) [19] and total synchronous fluorescence spectroscopy (TSFS) [20]. Three-dimensional EEM and TSFS spectra provide a spectral signature of the multiple fluorophores presents in a protein or a complex multi-fluorophore sample [21-23]. The primary advantages of TSFS over EEM measurements are to avoid the collection of Rayleigh scatter and that it is a somewhat quicker measurement. However, Rayleigh scatter does contain information about the physical nature of the sample and can be used to monitor particle formation such as aggregation [24].

Anisotropy resolved multidimensional emission spectroscopy (ARMES) combines anisotropy, MDF measurements, and chemometrics [25]. ARMES generates multidimensional datasets (excitation wavelength (λ_{ex}), emission wavelength (λ_{em}) or wavelength offset ($\Delta\lambda$), intensity (I), anisotropy (r)) and provides additional information with which one can characterize proteins and differentiate the emission of each fluorophore or a family of fluorophores. For multi-fluorophore proteins, anisotropy varies across the fluorescence emission space (plotted as an *aniso*-MDF map) because of the different fluorophores and the interactions (*e.g.* FRET) between them [22, 26]. The *aniso*-MDF maps are thus sensitive to structural change and this can be used as a different diagnostic measurement for assessing unfolding, refolding, and denaturation processes [25]. MDF data analysis requires the use of chemometric modelling techniques to try and resolve contributions from different fluorophores which can be used for analytical applications [27, 28]. For MDF/ARMES, multi-way decomposition methods, like multivariate curve resolution (MCR) [29, 30] and parallel factor analysis (PARAFAC) [31-33] are used to identify the spectral contribution of individual constituents. Care is needed with applying these methods to IFS because of the inherent non-linearity of the data, however, they are the most widely available tools and can produce useful outputs under specific conditions. This combination of anisotropy and MDF has previously enabled the differentiation of fluorophores with similar emission properties in complex mixtures. Anisotropy provides for fluorophore differentiation based on factors such as: FRET, rotational speed, hydrodynamic volume/molecular size, and for macromolecules the mobility/flexibility of the constituent fluorophores [25, 26, 34]. In proteins, all these factors are present, making the analysis of anisotropy changes a complicated process.

Previously we showed that ARMES of Human Serum Albumin (HSA) using MCR modelling yielded multiple components [25], however these studies used thin film polarizers with no transmission below 300 nm which affected the TSFS data structure. Further developments of ARMES to enable short (<300 nm) wavelength excitation [26] and validation measurements have shown that one can accurately recover individual fluorophore emission in the absence of inner filter effects (IFE) and FRET [35]. These early studies also undertook MCR analysis on all four polarization measurements, mainly in an effort to confirm that the chemometric modelling was robust [26, 36].

Here we investigate the use of ARMES to better characterize the fluorescence emission of a much more complex IgG protein in its native state, over a small temperature interval. It was hoped that the thermally induced variations over the 15−35°C range, might be small enough to avoid issues with non-linear changes in the spectral measurements (caused by large structural/FRET changes) yet enough to

induce sufficient fluorescence fluctuations for PARAFAC analysis. One might expect that different fluorophore populations should quench at slightly different rates as the temperature changed, this might be sufficient to discriminate, the internal versus the externally located Trp emission. This modelling of the native state emission is important because it serves as a baseline with which we can investigate processes such as unfolding and aggregation using ARMES and curve resolution methods.

2 Materials and methods

2.1 Materials

IgG from rabbit serum (≥95% essentially salt-free, lyophilized powder) was obtained from Sigma-Aldrich and used as received without further purification. SEC analysis of the three lots used for these studies showed that the monomer content was ~80±1% (data not shown). Sodium phosphate monobasic, sodium phosphate dibasic hepta-hydrate, and sodium chloride were used to prepare a 0.01 M Phosphate 0.150 M saline buffer (PBS) at pH 6.5±0.1 in high purity water (HPW) from Honeywell (HPLC grade). Except for the HPW, all the other materials were purchased from Sigma-Aldrich and used without further purification. Rabbit IgG (rIgG) solutions in PBS buffer were prepared in triplicate (1.1±0.2 mg mL^{-1}) using different vials of protein (but with the same lot number, SLBM2617V) and then membrane filtered (0.2 μm) using polyethersulfone (PES) Captiva Premium Syringe filters (Agilent). The three freshly prepared solutions had concentrations of: R1=1.3 mg mL^{-1}; R2=0.9 mg mL^{-1}, and R3=1.2 mg mL^{-1}, and these did not change after defrosting. Aliquots (sufficient for a single measurement) of each replicate solution were then dispensed into 1.5 mL Lobind tubes (Eppendorf) and stored at −70°C prior to use (over 13 weeks). All sample solution preparation was carried out in a laminar flow hood using aseptic techniques to minimize contamination. Prior to making spectroscopic measurements the samples were slowly defrosted overnight at 4−8°C, taking care to ensure that there were no ice crystals remaining before transfer into the cuvette.

2.2 Instrumentation and data collection

UV-Vis absorbance spectra (200−800 nm) were collected using a Cary 60 (Agilent) at a scan rate of 1200 nm min^{-1}. EEM, and ARMES, were performed using a Cary Eclipse fluorimeter (Agilent) fitted with bespoke dual wire grid polarizers [26] and a temperature-regulated multi-cell holder. All spectroscopic measurements were made in triplicate, using 10×2 mm pathlength quartz cuvettes (Lightpath Optical, UK). UV-Vis absorbance spectra were collected with a 2 mm pathlength; for the EEM measurements, samples were excited along the short axis (2 mm) and emission collected from the long axis (10 mm). Polarized EEM (pEEM) data were collected over an excitation and emission range of λ_{ex}=240−320 nm and λ_{em}=260−450 nm (2 nm step increments for both axis). Excitation and emission monochromators slit widths were 10 nm, the scan rate was 1200 nm min^{-1} and the photomultiplier tube (PMT) detector voltage was set to 650 V. All samples were measured using four polarizer settings: VH (vertical-horizontal), VV (vertical-vertical), HH (horizontal-horizontal), and HV (horizontal-vertical). The anisotropy (r) was calculated using the standard anisotropy formula [15], which was then used to construct the corresponding *aniso*-EEM maps. For the native state characterization, rIgG solutions were measured at 9 different temperatures (15°, 17°, 20°, 23°, 25°, 27°, 30°, 33°, and 35°C) with 5 minutes thermal equilibration between measurements and it took ~8 minutes to collect each pEEM spectrum.

Published Version: **DOI**: 10.1016/j.chemolab.2018.12.007.

2.3 Data analysis and chemometric methods

Data analysis was performed using the PLS_Toolbox ver. 8.2.1 (Eigenvector Research Inc.), MATLAB ver. 9.1.0 (The Mathworks Inc.), and in-house written program (FluorS). The EEM_{HV} and EEM_{HH} measurements were only used here to calculate the G-factor ($G = I_{HV}/I_{HH}$, Figure S2, SI) and thus correct the VH measurement to produce the corrected perpendicular emission [37]. The detector (and emission optics/monochromator) can have a different wavelength dependent sensitivity for vertically and horizontally polarized light and this must be corrected (Figure S3, SI) over the complete EEM spectrum [15, 37]. G factor corrected EEM_{VH} spectra are designated perpendicular polarization ($EEM_{\perp}$) and the EEM_{VV} spectra as parallel polarization ($EEM_{\parallel} = EEM_{VV}$). The total unpolarized EEM spectra (EEM_T) were calculated using $EEM_T = EEM_{\parallel}+2\times EEM_{\perp}$, and these served as controls for chemometric modelling [15, 37, 38].

EEM three-way arrays can be decomposed using bilinear methods such as MCR-ALS [39] or trilinear models like PARAFAC [33]. MCR-ALS offers the advantage to switch between bilinear, partial trilinear, and fully trilinear models [35], however, rotational ambiguities can be associated with the bilinear solutions [22, 23, 29, 30, 39, 40]. Thus, different constraints and augmentation modes can yield different solutions from the correct solution [30]. PARAFAC was preferred here due to the uniqueness of the solutions, which can be achieved with EEM data following the trilinear model [33] or when deviations from trilinearity are very small and not linked to the signal of the analyte to be determined [41]. Prior to PARAFAC, EEM data were pre-processed to minimize IFE, Rayleigh, and Raman scattering, all of which have very large adverse effects on anisotropy measurement accuracy [37]. The type of procedures used for pre-processing are very data/sample dependent and the sequence of steps could also be critical [33, 42, 43]. Furthermore, the use of interpolation of IFS spectra also needed to be carefully evaluated as there could be unwanted, unexpected spectral distortions induced. Here, multiple methods and combinations were evaluated for the specific issues associated with IgG emission, and Figure 1 shows the four best pre-processing sequences implemented.

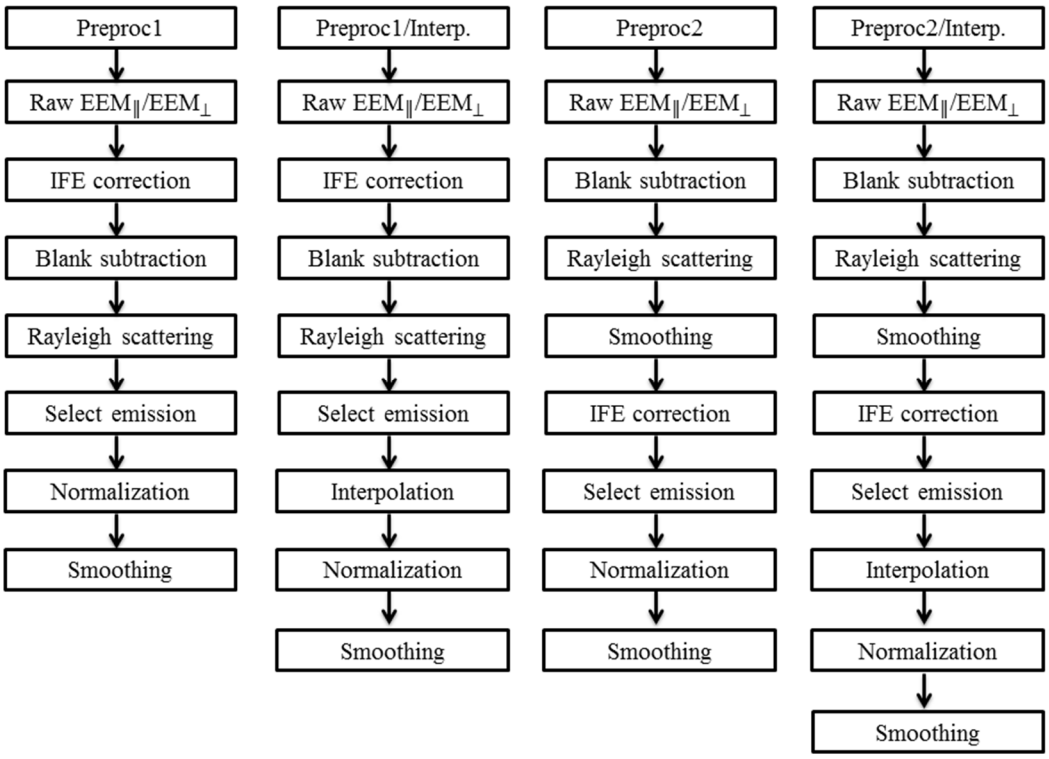

Figure 1: Schematic of the different sequences of pre-processing steps applied to pEEM data collected from the rIgG native state emission.

Raman and Rayleigh first order bands were present in the EEM data (Figure 2) and as scattered light [15] is non-trilinear it should be removed prior to PARAFAC analysis. Raman scatter was removed by subtracting a blank (PBS buffer) spectrum from the pEEM measurements (Figure S4C/S5B, SI). The first order Rayleigh scatter was modelled and corrected (Figure 2A/D) as previously described [26, 44].

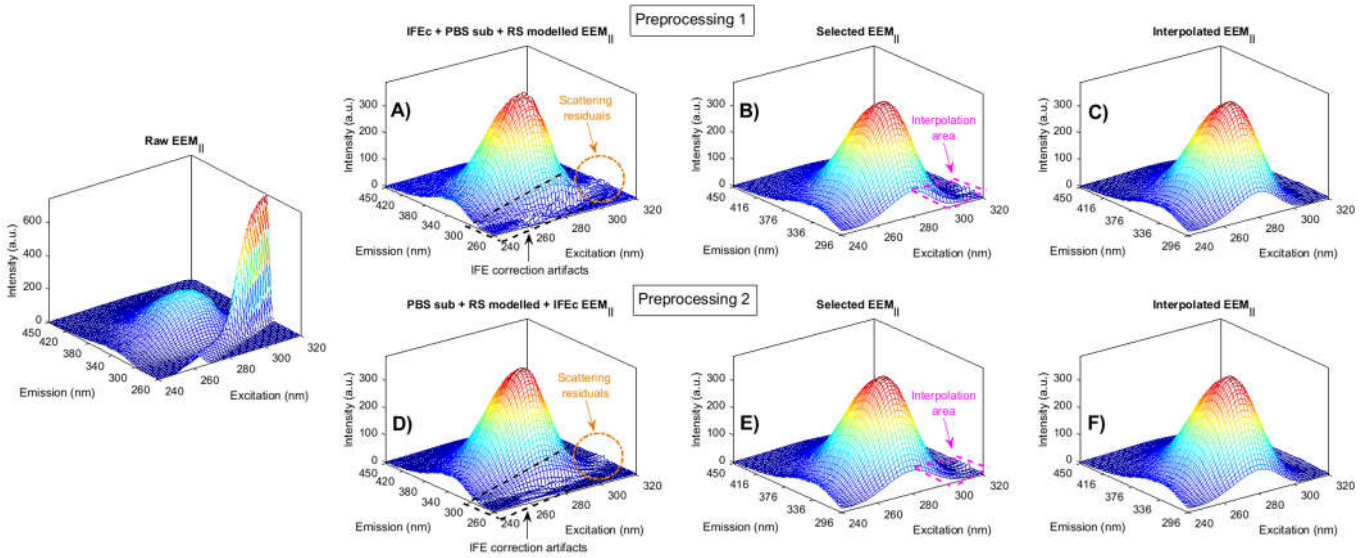

Figure 2: (Left) Raw EEM‖ spectra of rIgG native state measured at 20°C. The two different schemes for pre-processing: Preproc1 started with: (A) IFE correction (IFEc), followed by blank subtraction (PBS sub) and then Rayleigh scattering

removal. Preproc2 started with: (D) blank subtracted, followed by RS removal, and the IFE correction. Both sets of corrected data were the cut at λ_{em} 296 nm to remove residual scattering and noise (B/E) before being interpolated to remove most of the remaining residual light scatter and finally smoothed (C/F).

The EEM data required IFE correction because of the high optical density (A_{280} =0.32±0.05, 2 mm pathlength, Figure S6, SI) of the protein solutions [45, 46]. An absorbance-based correction (Equation 1) [15] was used: the measured absorbance (A_λ) at each excitation (λ_{ex}) and emission (λ_{em}) wavelength combination was used to convert the observed fluorescence intensity (F^{obs}) to a corrected fluorescence intensity (F^{corr}):

$$F^{corr}_{\lambda ex,\lambda em} = F^{obs}_{\lambda ex,\lambda em} \times 10^{\left(\frac{A_{\lambda ex}+A_{\lambda em}}{2}\right)} \text{ ; if } F^{obs}_{\lambda ex,\lambda em} > LOR\ F_{\lambda em,\lambda ex} \qquad \textbf{Equation 1.}$$

Only the spectral co-ordinates which had fluorescence intensities that were above the limit of reporting (LOR, $LOR\ F_{\lambda em,\lambda ex} = F_{blank(\lambda em,\lambda ex)} + 10 \times SD(F_{blank(\lambda em,\lambda ex)})$) [45] were corrected. The LOR at each $\lambda_{em}/\lambda_{ex}$ coordinate was calculated for each polarized measurement from the standard deviation of 10 blank replicate measurements (Figure S7, SI). IFE correction was critical here for PARAFAC resolution and anisotropy calculations because the polarized measurements were much weaker than normal, unpolarized EEM measurements [25].

IFE correction introduced some artefacts related to amplified noise in the λ_{em} <292 nm region where emission was weak. To solve this, the spectra were edited to eliminate this region, yielding new data, with λ_{em}≥296 nm (Figure 2B/E). This removed area was mostly weak Tyr emission and the Trp emission blue edge (at short wavelengths) [15, 47]. The other pre-processing steps were to remove the residual noise in the Rayleigh scatter region from the EEM by interpolation [43] and to reduce unwanted noise using Savitzky-Golay smoothing using a second-order polynomial with a 15-point window size (Figure 2C/F) [48]. These pre-processed pEEM spectra were used to calculate the corresponding anisotropy (r) at each $\lambda_{ex}/\lambda_{em}$ coordinate (Equation 2) [37]. This was then used to generate a multidimensional data matrix ($\lambda_{ex} \times \lambda_{em} \times r$) over the full emission space (*aniso*-EEM map):

$$\bar{r}_{(\lambda ex,\lambda em)} = \frac{EEM_{\parallel(\lambda ex,\lambda em)} - EEM_{\perp(\lambda ex,\lambda em)}}{EEM_{\parallel(\lambda ex,\lambda em)} + 2 \times EEM_{\perp(\lambda ex,\lambda em)}} \qquad \textbf{Equation 2.}$$

For PARAFAC, the pre-processed EEM_T, and $EEM_\parallel/EEM_\perp$ were arranged in a three-dimensional structure (X) of size, 27 samples × 78 λ_{em} × 41 λ_{ex} (Figure 2B/E), and normalized by peak maximum [31]. The datasets were normalized to remove intensity differences due to small concentration differences during solution preparation and day-to-day fluctuations in excitation light intensity. Normalization focuses the model on purely structural variations of the protein rather than the signal, magnitude. This should increase the probability that the weaker fluorophore contributions might be resolved. In any case, the PARAFAC models for the non-normalized and normalized datasets were the same, but with a slightly improvement in model validation (especially RSD of the score values) for the normalized datasets. Several methods were used for determining the correct number of PARAFAC factors: CORe CONsistency DIAgnostic test (CONCORDIA) [49], the percentage of variance explained by the model (Table S1, SI), and visual inspection of the recovered spectral profile and residuals. Non-negative constraints for all modes (samples and both emission and excitation profiles) were applied and

PARAFAC initialization was made by selecting the best-fitting model from several trial models fitted using a low number of iterations. Validation of spectral deconvolution results were performed using split-half analysis [33].

First, the $EEM_{\parallel}$, $EEM_{\perp}$, and EEM_T datasets were analysed by PARAFAC to see if: (a) the different pre-processing schemes had an impact; (b) the use of interpolation distorted the data; (c) different fluorophores could be resolved; and (d) if there were differences in the recovered loadings (spectra) for the differently polarized emission. This was a long and complex iterative process to carefully select the best pre-processing method for PARAFAC analysis of proteins which unlike the small molecule case [35], there is no *a-priori* knowledge about the precise component profile to be recovered other than empirical knowledge of the peak positions for Tyr and Trp emission.

3 Results and discussion

3.1 2D spectral analysis

2D emission wavelength plots were used to quickly assess the degree of spectral variation generated over the temperature range and determine if there were significant differences in Trp and Tyr emission, and Tyr-to-Trp FRET [15, 50]. The difference between the emission spectra excited at 270 (Trp and Tyr excited) and 296 nm (mainly Trp excited) should represent the directly excited Tyr emission (i.e. the fraction which does not undergo FRET with the numerous Trp acceptors) [51-53]. The gross difference plots showed some evidence for weak Tyr emission overlapped with Trp emission (λ_{em} ~320 nm), in the unpolarized EEM_T datasets (Figure 3).

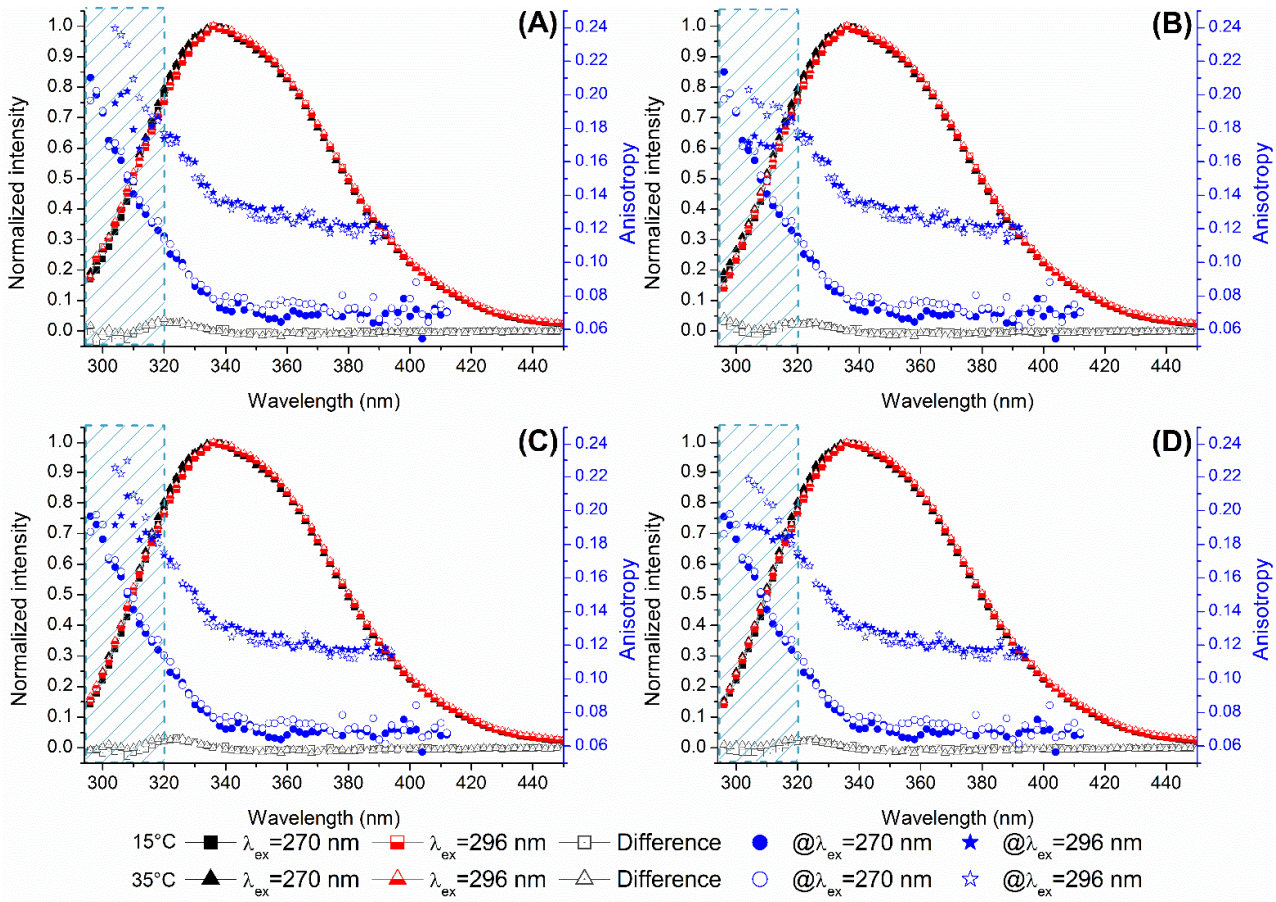

Figure 3: Normalized EEM_T emission spectra of rIgG excited at λ_{ex} 270 and 296 nm and the difference spectra (= λ_{ex} 270 − λ_{ex} 296) of the rIgG native state corrected with: (A) Preproc1, (B) Preproc1/Interpolated, (C) Preproc2, and (D) Preproc2/Interpolated, at two different temperatures (15° and 35°C), overlaid with the emission anisotropy at λ_{ex} 270 and 296 nm (blue circles and stars). The shaded boxes represent the spectral region affected by residual noise.

There was minimal change in spectral profile over the 15−35ºC temperature range, with a relative standard deviation (RSD) of <6.1% and <5.7% for Preproc1 and Preproc2, respectively. This confirmed that the rIgG structure did not change significantly and thus could be considered to be in its native form throughout this temperature range. The anisotropy plots did not change much with the different pre-processing methods (Figure 3), however there was a small change between the anisotropy values at the blue edge, with an RSD <3.8% and <7.4% for the anisotropy values with λ_{ex} 270 and 296 nm, respectively. This variance in anisotropy at the blue edge (λ_{em}<320 nm) was related to residual noise from the Rayleigh light scatter. Preproc2 (Figure 3C) better removed the artefact created by IFE correction compared to Preproc1 (Figure 3A), but residual noise was still present as shown by the high anisotropy values. The use of interpolation removed this residual noise without affecting the anisotropy outside of the scattering affected zones (Figure 3B/D). However, there were noticeable differences with the 270 nm excitation, which means that the values in this region were suspect (*vide infra*).

3.2 *Aniso*-EEM maps

However, the use of single excitation wavelength spectra omits a lot of potentially useful information and while the selection of excitation wavelengths at 270 and 296 nm showed changes at the blue edge, it might miss subtle red edge (at longer wavelengths) effects for example [54]. This is the rationale for examining the full emission space. The *aniso*-EEM maps for rIgG were heterogeneous with the

variation across the emission space being generated by multiple factors such as: the type and number of fluorophores, fluorophore location within the protein, differences in fluorophore motility, variations in intra-molecular FRET, and differences in the physicochemical environments of the fluorophores. A visual inspection of the *aniso*-EEM maps for the different pre-processing methods (Figures 4/5) at various temperatures showed a small change for λ_{em}>336 nm. Neither pre-processing method affected the Trp emission region (λ_{em}~330−350 nm) however, visual inspection of the *aniso*-EEM maps in the shorter emission wavelengths (λ_{em}<336 nm) showed a clear difference between the pre-processing methods. The Preproc1 corrected *aniso*-EEM maps (Figure 4A−C) showed a more irregular contour compared to those generated using Preproc2 (Figure 5A−C). This was due to the residual shot noise from Rayleigh scatter being amplified in the data corrected using Preproc1. The maximum anisotropy values were higher and more variable for Preproc1 than Preproc2 (Figure S8, SI), with an RSD of 8.90% and 3.88% (for triplicate measurements at all temperatures). We can conclude therefore that Preproc2 (Figure 2E) was more efficient removing residual scattered light and did not amplify noise and IFE correction artefacts as much as Preproc1 (Figure 2B). One should implement the subtractive elements (Raman and Rayleigh corrections) prior to multiplicative elements (IFE correction) otherwise one gets increased noise contributions. This issue is particularly important in the UV (λ<250 nm) where system response changes and the fluorescence emission signal is weak.

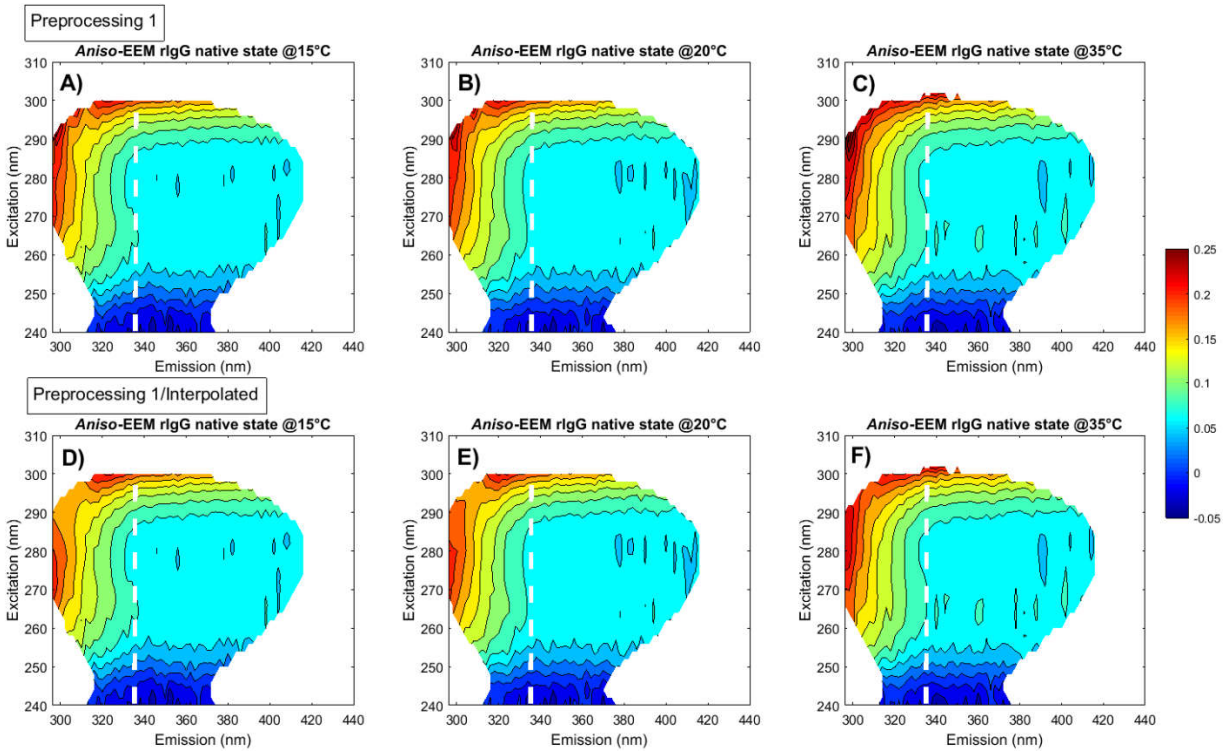

Figure 4: *Aniso*-EEM maps for rIgG measured at (A/D) 15°C, (B/E) 20°C, and (C/F) 35°C corrected with (Top) Preproc1 and (Bottom) Preproc1/Interp. The dashed lines show the λ_{em} =336 nm excitation line. The colour bar on the right represents the anisotropy scale.

Incomplete light scatter removal produces higher anisotropy values (higher EEM‖ intensities). To try and completely remove the residual scatter, interpolation was used. The inspection of the *aniso*-EEM maps for Preproc1/Interp. showed a reduction in the contour irregularity and lower anisotropy values in the scatter area (RSD=4.90%, for triplicate measurements at all temperatures) in comparison with the

non-interpolated Preproc1 (Figure 4). The differences between the *aniso*-EEM maps for the Preproc2/Interp. (RSD=3.15%, triplicate measurements at all temperatures) and non-interpolated Preproc2 (Figure 5) were less significant. The maximum anisotropy values (measured over the whole map) decreased between the non-interpolated and the interpolated pre-processed cases (Figure S8, SI). These differences in maximum anisotropy values between the Preproc1 and Preproc1/Interp. indicated that interpolation was efficient at removing the residual noise. The small differences between the maximum anisotropy values of Preproc2 and Preproc2/Interp. showed that this pre-processing method was more efficiently removing Rayleigh scatter and noise from the data.

However, care must be exercised here because proving that interpolation does not distort the true emission is not easy in FRET dominated systems like proteins. In the ideal small molecule case where no FRET occurs then it is possible to verify that the corrected spectra matches the individual components or mixtures thereof. Therefore, one has to ensure that whichever pre-processing/interpolation method is selected that this is fixed throughout the analysis, and that the anisotropy values in these regions be understood to be estimates rather than accurate values.

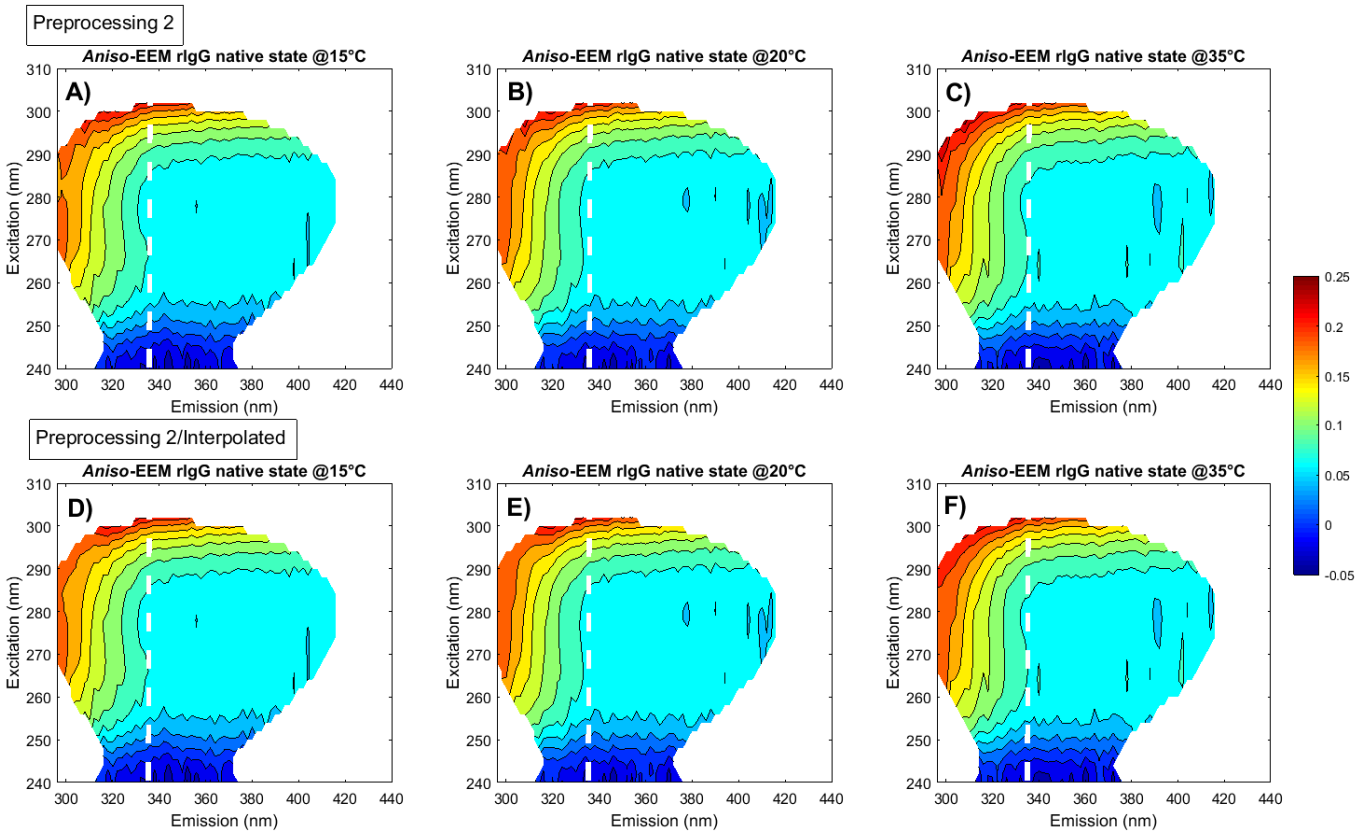

Figure 5: *Aniso*-EEM maps for rIgG measured at (A/D) 15°C, (B/E) 20°C, and (C/F) 35°C corrected with (top) Preproc2 and (bottom) Preproc2/Interp. The dashed lines show the λ_{em} =336 nm excitation line. The colour bar on the right represents the anisotropy scale.

Interpolation improved scattering/noise removal as confirmed by the reduction in maximum anisotropy values (Figure S8, SI). The mean anisotropy values over the full emission space did not change with the different pre-processing methods: an RSD of 7.67% and 7.04% for Preproc1 and Preproc2, and 7.79% and 7.03% for Preproc1/Interp. and Preproc2/Interp. (for triplicate measurements

at all temperatures). This indicated that overall, the degree of structural change was small and as there were no differences in the mean anisotropy between pre-processing with and without interpolation, one might assume that the interpolation did not affect the data. However, the use of mean anisotropy values for this type of assessment is not correct as the anisotropy intrinsically varies over the full emission space and thus alternative assessment methods which can quantify the degree of change were required.

A similarity index (SimI) [55] was calculated (using the *aniso*-EEM map from the first replicate measurement at 15ºC as the reference spectrum) for all the samples (Figure 6). This showed that the *aniso*-EEM maps using Preproc2 (RSD=22.06%), Preproc2/Interp. (RSD=21.50%) were more similar to each other than the *aniso*-EEM maps for Preproc1 and Preproc1/Interp. (RSD=35.71%) which can be largely ascribed to the noise issues from the scatter contamination.

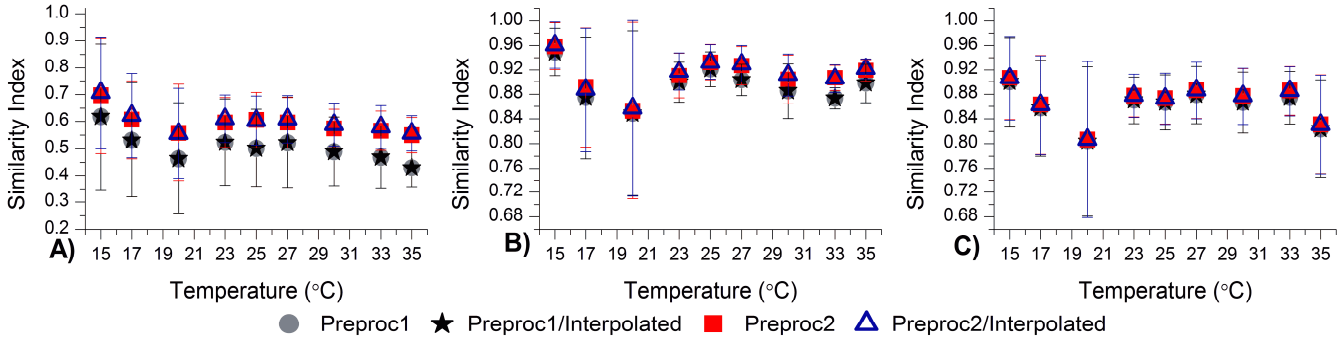

Figure 6: SimI values calculated between the *aniso*-EEM for each pre-processing method for: (A) the full emission space, (B) the area related to Tyr emission ($\lambda_{ex}/\lambda_{em}$=270−290/300−320 nm); and (C) the area related to Trp ($\lambda_{ex}/\lambda_{em}$=280−300/320−360 nm) emission. A SimI value of one indicates identical maps. Error bars generated from the standard deviation from triplicate measurements of the independent samples.

The small dip at 20°C (Figure 6) is a real effect since the data were collected on three different days, at approximately the same time using identical measurement settings, and each stock solution was prepared from a different source vial (but with the same lot number). This dip (and increase in the error bars) was possibly due to a change in local motion at 20°C, but at present we have no clear evidence to support this [56, 57]. A reduction in flexibility could cause measurable changes in polarization, but probably not much in terms of overall emission profile. As the temperature increases above 23°C up to 35°C, SimI values remained constant, indicating a stable structure. This requires further investigation as the protein was polyclonal in origin with only ~80% monomer and rabbit IgG composition is known to vary [58].

To better assess the changes in Tyr/Trp emission in the *aniso*-EEM maps (Figures 4/5) two areas were selected (Figure S10, SI): Tyr ($\lambda_{ex}/\lambda_{em}$=270−290/300−320 nm) and Trp ($\lambda_{ex}/\lambda_{em}$=280−300/320−360 nm). Here the variation was considerably smaller (Figure 6B/C) with very small differences between the *aniso*-EEM maps (RSD~8.60%) for the Trp region. Likewise, the Tyr region did not show any significant differences in the *aniso*-EEM maps (RSD~7.65%). SimI analysis of specific Tyr and Trp emission regions showed that there was no difference in the *aniso*-maps due to the pre-processing methods outside of the Rayleigh scattering region. Overall, the poor discrimination of *aniso*-EEM map analysis can be attributed to the greater errors associated with anisotropy measurements. This coupled with the small structural changes and the relatively high noise spectral measurements implemented here make it a less useful method for assessing small changes in IgG structure.

3.3 PARAFAC

Visual inspection and SimI analysis of *aniso*-EEM maps (Figures 4/5) suggested that we had observed some Trp emission changes caused by temperature induced variations in the rIgG structure. It was hoped that sufficient spectral variance had been induced so as to enable PARAFAC to resolve individual fluorophore emissions from the rIgG native state in a similar fashion to previously reported for HSA [59]. We know that protein emission does not vary linearly because of FRET and when this occurs then the assumptions of variability, trilinearity, and additivity required [33] for successful and chemically meaningful PARAFAC analysis do not hold. However, for small structural variations it might be reasonable to expect that the structural changes were sufficient to induce significant emission intensity fluctuations (via varying quenching rates for different fluorophores) without significant changes in spectral shape. PARAFAC models were generated from pre-processed $EEM_{\parallel}$, $EEM_{\perp}$, and EEM_T data of all samples (9 temperatures × triplicate measurements). From an rIgG structure assessment (Figure S1, SI), one might expect to recover at least three components, one from Tyr, a second from Trp located in more hydrophobic environments (λ_{em}~330 nm), and a third one from more solvent exposed Trp (λ_{em}>340 nm). In addition to environmental factors, Trp emission in IgG is generated via three photochemical processes: *(i)* direct excitation of, and emission from the excited state, should produce emission with a high anisotropy, *(ii)* homo-FRET from other Trp fluorophores, should result in lower anisotropy [60], and *(iii)* hetero-FRET from Tyr, again producing low anisotropy. Therefore, one might expect to see this reflected in the presence of one or two additional components with an appreciable score.

Even though rIgG contains ~50 Tyr and ~24 Trp fluorophores, PARAFAC only recovered two components (PFC1 and PFC2) from the EEM data (Table 1, Figure 7) and the contribution of the second component was very small, and very sensitive to pre-processing. This was largely based more on differences in the excitation spectra. Increasing the component number up to four (Table S1, SI) and analysis of the residuals produced no better fit models. For all the PARAFAC models the first component resolved was virtually identical for all polarizations (SimI = 0.9494, RSD = 1.78%). This coupled with the facts that the emission was relatively depolarized (~0.1 for most of the emission), and that the excitation anisotropy spectra (see below) were distinctive indicated that it originated mostly from FRET rather than direct excitation/emission of the fluorophores. There were several reasons why only two components were recovered: *(i)* the structural changes and thus emission changes over the temperature range sampled were too small; *(ii)* the Tyr-to-Trp FRET was very strong and effectively constant over the 15−35°C temperature range; *(iii)* the emission spectra of the different Trp populations overlapped and the observed emission spectrum represented an average of buried and partially exposed Trp fluorophores (λ_{em}~336 nm).

Table 1: Comparison of the model parameters and components obtained for the normalized polarized $EEM_{\parallel}$, $EEM_{\perp}$, and unpolarized EEM_T PARAFAC models of the rIgG native state corrected with the different pre-processing methods.

	Preproc1			Preproc1/Interp.			Preproc2			Preproc2/Interp.		
	$EEM_{\parallel}$	**$EEM_{\perp}$**	**EEM_T**	**$EEM_{\parallel}$**	**$EEM_{\perp}$**	**EEM_T**	**$EEM_{\parallel}$**	**$EEM_{\perp}$**	**EEM_T**	**$EEM_{\parallel}$**	**$EEM_{\perp}$**	**EEM_T**
C1 $\lambda_{ex}/\lambda_{em}$ (nm)	280/336	280/336	278/336	280/336	280/336	278/336	280/336	278/336	280/336	278/336	278/336	278/336
C1 Fit model (%)	99.73	99.70	99.85	98.74	99.71	99.65	99.75	99.74	99.85	99.34	99.75	99.84
C2 $\lambda_{ex}/\lambda_{em}$ (nm)	296/342	296/346	296/346	298/336	296/346	298/342	296/342	296/346	298/346	298/338	296/346	298/346
C2 Fit model (%)	**0.27**	**0.30**	**0.15**	**1.26**	**0.29**	**0.35**	**0.12**	**0.26**	**0.15**	**0.66**	**0.25**	**0.16**
Variance explained (%)	99.97	99.99	99.99	99.98	99.99	99.98	99.98	99.99	99.98	99.98	99.99	99.98
CONCOR DIA	95.22	88.71	97.02	96.92	86.80	69.21	96.84	91.53	96.61	57.96	88.43	95.76
Split-half analysis (%)	99.13	99.67	99.74	98.39	99.74	99.82	99.14	99.64	99.82	99.57	99.67	99.86

For the freely diffusing small molecule case, the excitation spectrum of Tyr anisotropy should be positive from λ_{ex} =260 nm, with an increase up to 290 nm [61, 62]. For Trp, the excitation anisotropy spectra should not be constant, due to the overlapping excitation of the two transition states. A minimum anisotropy value at ~λ_{ex} 290 nm should be observed when the maximum excitation is due to the ^1L_b excited state, and a maximum at ~λ_{ex} 300 nm indicates excitation of the ^1L_a excited state of Trp [15, 37, 38, 61-63]. From an analysis of the loadings it was clear that PFC1 was the same for all pre-processing methods (Figure 7) and represented a composite signal from both Trp and Tyr fluorophores. In all the cases the excitation spectrum was very similar to that of Tyr [61, 62], whereas the emission was that of Trp. Therefore, we can conclude that this component largely represents the hetero-FRET Tyr-to-Trp process, with probably a minor contribution from directly excited Tyr emission at the blue edge of the emission (in the region where the anisotropy increases). The fact that PFC1 is largely due to hetero-FRET would also explain the low calculated anisotropy recovered (~0.05 for λ_{em}>340 nm). The slightly higher anisotropy values for the non-interpolated pre-processing (Figure 7A/C) EEM PFC1 might be attributed to the presence of noise (i.e. the Rayleigh shot noise) in the spectral data which also impacted on component recovery [15].

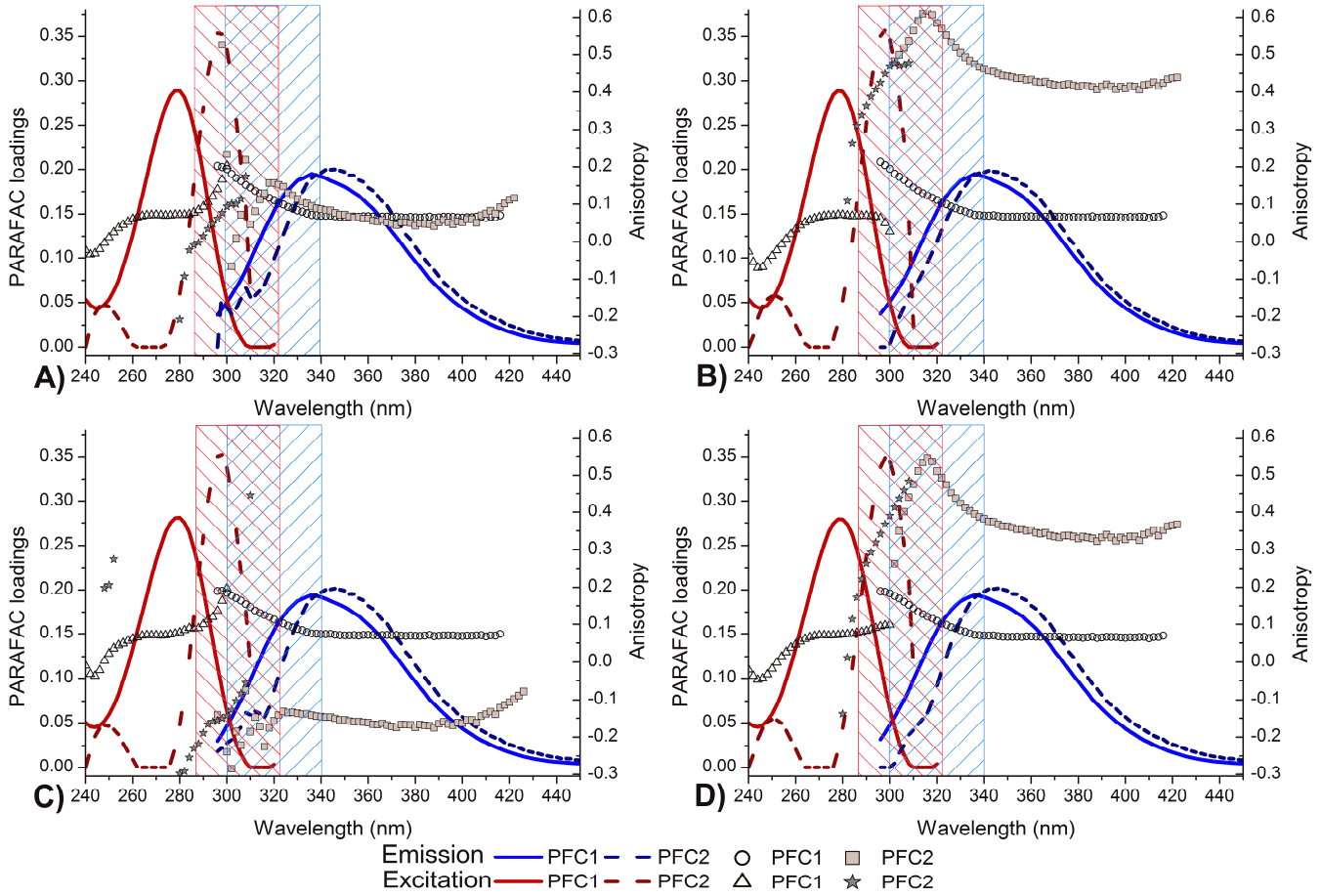

Figure 7: Comparison of PARAFAC modelling of the rIgG native structure for the EEM_T datasets with the different pre-processing methods. PFC1 and PFC2 (A) Preproc1, (B) Preproc1/Interp., (C) Preproc2, and (D) Preproc2/Interp. emission and excitation profiles recovered for unpolarized EEM_T, overlaid with the component anisotropy recovered at 20ºC. The anisotropy values were calculated for each component at $\lambda_{ex/em}$= 280/336 and 298/346 for PFC1 and PFC2 respectively. The shaded boxes represent the spectral regions most affected by scatter in the EEM.

The very weak second PARAFAC component, while definitely present, was not clearly resolved, and its properties (e.g. anisotropy) was very sensitive to pre-processing. This makes it hard to unambiguously assign this to any specific emission or use for quantitative assessments. However, it does look like that PFC2 was related to Trp emission that originated from direct excitation because of the high anisotropy for PFC2 at longer wavelengths and the excitation and emission wavelengths recovered (Table 1). This would suggest that the Trp residues that give rise to this component were most likely located in the hyper variable Fab region. We do have to note however that interpolation had a big impact on the recovered anisotropy at short emission wavelengths (Figure 7) because of the effects on $EEM_{\parallel}$ (Table 1). Interpolation generated a ~5-fold increase in the PFC2 scores, which can be ascribed to the fact that the scatter signal in $EEM_{\parallel}$ was much greater than $EEM_{\perp}$ or EEM_T. This means that the remaining shot noise was very significant and was indistinguishable from emission and was thus included in the data for PARAFAC. This then also contributed to the increased anisotropy in these regions and a lot of the variability in the *aniso*-EEM maps. This meant that the component anisotropy recovered for <340 nm was unreliable, but at the longer emission wavelengths it should be sensible.

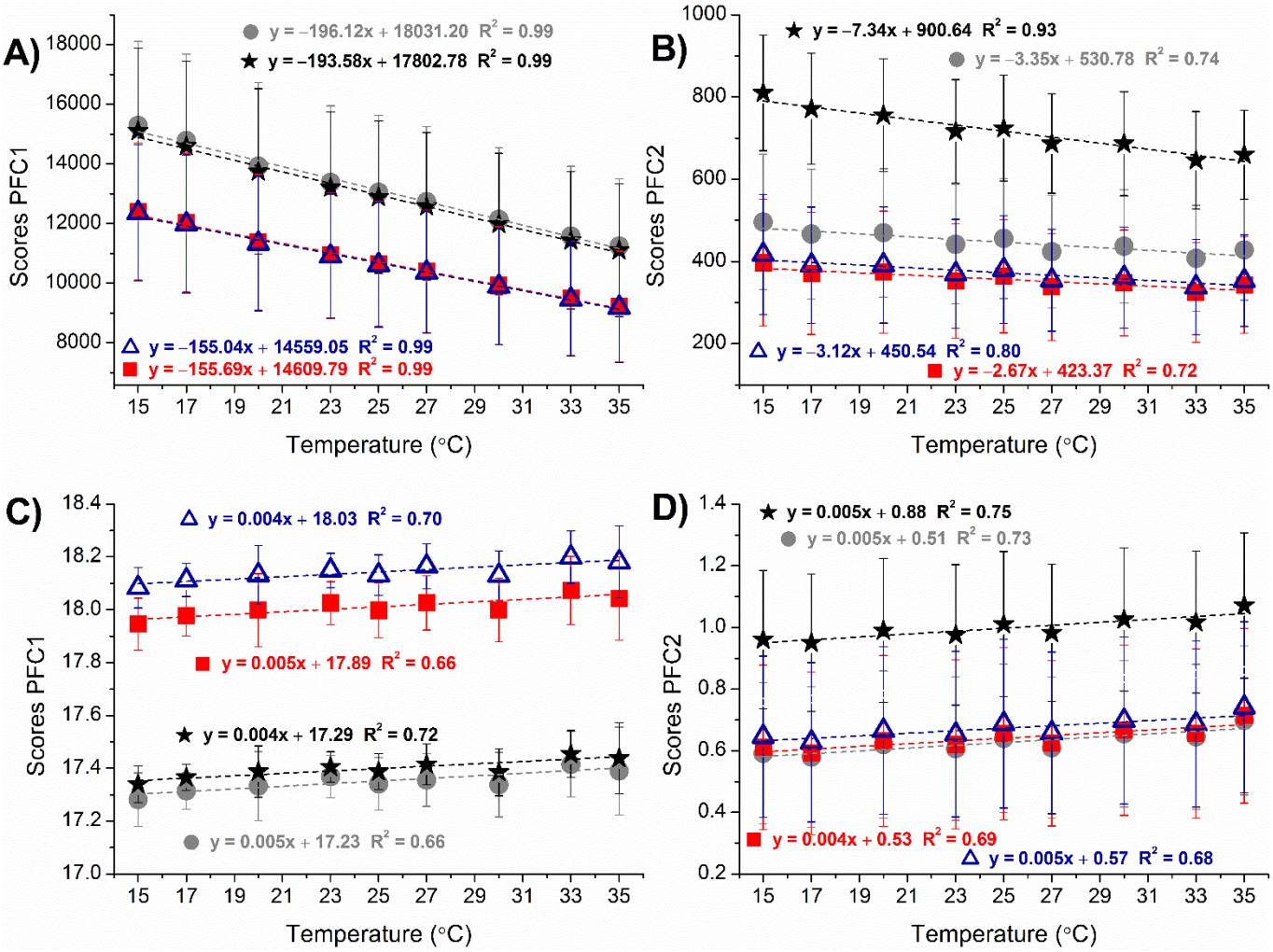

Figure 8: Scores plots of the two-component PARAFAC models for the non-normalised (top) and normalized (bottom) unpolarized rIgG EEM_T datasets. (Left) PFC1 and (Right) PFC2 scores for the various pre-processing methods used to correct the data. The grey circles and black stars Preproc1/Preproc1-Interpolated respectively, while the red squares and blue triangles are Preproc2/Preproc2-Interpolated respectively. P values for the regression fits in A & B were <0.05 indicating that the changes were statistically significant. For C& D the regression fits had P-values of <0.001.

Because the differences between the different polarized datasets were all small and with low scores (Figure 8, and Figure S12, SI), and since the data was relatively noisy, this limited our ability to identify any real photophysical or structural changes. However, if the PARAFAC modelling process was robust one might expect that the results from the different pre-processing should yield the exact same result within reason. Indeed, all four pre-processing methods yielded virtually the same PARAFAC solutions (Figure S11, SI), with differences in the model validation (Table 1). Most importantly, all the significant differences in PARAFAC loadings were within the interpolated area (Figure 7). For the normalized unpolarized EEM_T data the scores of both PARAFAC models' components showed no change in scores with temperature (Figure 8, and Figure S12, SI) indicating that there were no significant change in spectral shape (and thus structure). For the non-normalised EEM_T data, the scores decreased linearly for both components indicating that the major change in emission properties was due to simple fluorescence quenching due to increasing thermal motion [11, 17, 64].

4 Conclusions

For rIgG the fluorescence changes over the 15–35 °C temperature range were mostly attributable to simple emission quenching with very little change in spectral shape. This indicated that the native state structure was preserved in this region and thus there were minimal changes in FRET. In the rIgG native state, most Trp fluorophores are located within the structure (higher quantum yield, more blue emitting) with only a few being partially solvent exposed (lower quantum yield, more red emitting) [15]. This would result in the majority of Trp emission coming from these internal Trp residues and therefore we might not be able to discriminate the different Trp populations. Likewise, with Tyr, the lower quantum yields and extensive Tyr-to-Trp FRET will reduce emission intensity to such an extent that one might not be able to resolve the Tyr emission. This was the case here and PARAFAC only recovered one major and one minor component. We suggest that the observed component discrimination was largely based on the difference in Trp excitation mechanisms that is, between direct excitation/emission (including homo-FRET), and that originating via energy transfer from Tyr [15, 65, 66]. However, the fit of the second component were low (<1.3%) and very sensitive to the precise sequence of processing steps.

The inability to extract any more components was due to a combination of factors. First, there were too many Trp fluorophores (>20) in different positions within the protein, and this generated a distribution of overlapping emission spectra rather than discrete spectra which is a problem for PARAFAC (or MCR). Second, because the protein structure did not change significantly, there was no major changes in Trp environment which kept the Tyr-to-Trp FRET rates constant and thus there were minimal changes in component ratios. Third, despite the larger number of Tyr residues present, its lower quantum yield, and the large Tyr-to-Trp energy transfer rates reduced Tyr emission intensity to very low levels [15, 50]. Fourth, the use of UV transparent wire grid polarizers [26] ensured that the emission data recorded was different to the red-edge excited TSFS data collected previously for HSA [59], and this may also have some effect on component resolution. Finally, as the only significant measured changes were thermal quenching related and were apparently the same for all fluorophores, this produced a high degree of co-linearity, thus no mechanism to break the linear dependencies, and so no additional components.

For the rIgG EEM data, for all the correction methods implemented, residual Rayleigh scattering (probably the shot noise), and artefacts induced by IFE correction caused significant issues, and in cases made the PARAFAC results less reliable. It was better to implement subtraction-based corrections (blank subtraction and scattering correction) and smoothing before any multiplication-based steps (IFE correction). The use of interpolation in a small spectral region had minimal impact on the components recovered and was shown to apparently improve some aspects of PARAFAC modelling. However, it was obvious that overlap between the emission blue edge with residual noise (shot noise from the Rayleigh scatter) was a critical factor (Figure S11, SI). This can be easily explained once we take into consideration the 10 nm slit widths of used here, and the fact that the scatter became much stronger for λ_{ex}>280 nm, yielding a heavily scatter contaminated $\lambda_{ex}/\lambda_{em}$=280–320/290–330 nm region.

The presence of relatively high shot noise signal associated with this strong Rayleigh scatter in the parallel polarization measurements caused problems because after correction there was a relatively large (compared to other regions in the EEM) shot noise signal that had an average signal greater than the baseline and thus was indistinguishable from fluorescence. This distorted the EEM$_{\parallel}$ spectra which in turn affected anisotropy values in this region and PARAFAC modelling (Table 1). Thus, the relatively

high noise signal intensities, combined with Tyr and Trp emission overlap made it difficult to accurately recover the emission blue edge. It was clear that if we want to more accurately resolve emission components from EEM data then we need either to collect data with much less Rayleigh scatter or use a denoising method that can handle the heterogenous noise pattern in the EEM space. The first can be achieved using more expensive spectrometers with better stray light rejection (double emission monochromators) and/or the use of smaller emission slits, neither of which may not always be practical or feasible with the standard fluorimeters found in most laboratories.

In conclusion, this study has provided a starting point from which we can explore the use of PARAFAC for the analysis of larger structural changes in IgG type proteins such as unfolding and aggregation. In particular the fact that PARAFAC potentially discriminated Trp emission on the basis of whether or not it was directly excited or excited via FRET from Tyr is potentially very useful for explaining changes in IgG emission spectral profiles.

5 Supplemental information available

Supporting information is available which provides additional spectral data further details on the chemometric analysis.

6 Acknowledgements

This publication has emanated from research supported in part by a research grant from Science Foundation Ireland (SFI) and is co-funded under the European Regional Development Fund under Grand number (14/IA/2282, *Advanced Analytics for Biological Therapeutic Manufacture*, to AGR). We also thank Agilent Technologies (Mulgrave Victoria, Australia) for the loan of a fluorescence spectrometer.

7 References

[1] J.M. Reichert, Marketed therapeutic antibodies compendium, Mabs, 4 (2012) 413-415.

[2] D.M. Ecker, S.D. Jones, H.L. Levine, The therapeutic monoclonal antibody market, Mabs, 7 (2015) 9-14.

[3] K.M. Murphy, C. Weaver, Janeway's Immunobiology, 9th edition. ed., New York, NY : Garland Science/Taylor & Francis Group, LLC2016.

[4] J.G. Salfeld, Isotype selection in antibody engineering, Nat. Biotechnol., 25 (2007) 1369-1372.

[5] P.-P. Pastoret, Handbook of vertebrate immunology, San Diego ; London : Academic Press, San Diego ; London, 1998.

[6] A. Pinheiro, F. Neves, A.L. de Matos, J. Abrantes, W. van der Loo, R. Mage, P.J. Esteves, An overview of the lagomorph immune system and its genetic diversity, Immunogenetics, 68 (2016) 83-107.

[7] K.L. Knight, R.C. Burnett, J.M. McNicholas, Organization and Polymorphism of Rabbit Immunoglobulin Heavy-Chain Genes, J. Immunol., 134 (1985) 1245-1250.

[8] R.M. Ionescu, J. Vlasak, C. Price, M. Kirchmeier, Contribution of variable domains to the stability of humanized IgG1 monoclonal antibodies, J. Pharm. Sci., 97 (2008) 1414-1426.

[9] P. Arosio, S. Rima, M. Morbidelli, Aggregation Mechanism of an IgG2 and two IgG1 Monoclonal Antibodies at low pH: From Oligomers to Larger Aggregates, Pharm. Res., 30 (2013) 641-654.

[10] B. Sharma, Immunogenicity of therapeutic proteins. Part 1: Impact of product handling, Biotechnol. Adv., 25 (2007) 310-317.

[11] E. Cerasoli, J. Ravi, T. Garfagnini, S. Gnaniah, D. le Pevelen, G.E. Tranter, Temperature denaturation and aggregation of a multi-domain protein (IgG1) investigated with an array of complementary biophysical methods, Anal. Bioanal. Chem., 406 (2014) 6577-6586.

[12] C.H. Li, X. Nguyen, L. Narhi, L. Chemmalil, E. Towers, S. Muzammil, J. Gabrielson, Y. Jiang, Applications of circular dichroism (CD) for structural analysis of proteins: qualification of near- and far-UV CD for protein higher order structural analysis, J. Pharm. Sci., 100 (2011) 4642-4654.

[13] B. Ranjbar, P. Gill, Circular Dichroism Techniques: Biomolecular and Nanostructural Analyses- A Review, Chemical Biology & Drug Design, 74 (2009) 101-120.

[14] S. Zolls, R. Tantipolphan, M. Wiggenhorn, G. Winter, W. Jiskoot, W. Friess, A. Hawe, Particles in therapeutic protein formulations, Part 1: Overview of analytical methods, J. Pharm. Sci., 101 (2012) 914-935.

[15] J.R. Lakowicz, Principles of Fluorescence Spectroscopy, 3rd Edition ed., Springer, New York, 2006.

[16] K. Wiberg, A. Sterner-Molin, S.P. Jacobsson, Simultaneous determination of albumin and immunoglobulin G with fluorescence spectroscopy and multivariate calibration, Talanta, 62 (2004) 567-574.

[17] P. Garidel, M. Hegyi, S. Bassarab, M. Weichel, A rapid, sensitive and economical assessment of monoclonal antibody conformational stability by intrinsic tryptophan fluorescence spectroscopy, Biotechnology Journal, 3 (2008) 1201-1211.

[18] L. Liu, L.J. Braun, W. Wang, T.W. Randolph, J.F. Carpenter, Freezing-Induced Perturbation of Tertiary Structure of a Monoclonal Antibody, J. Pharm. Sci., 103 (2014) 1979-1986.

[19] I.M. Warner, G.D. Christian, E.R. Davidson, J.B. Callis, Analysis of Multicomponent Fluorescence Data, Anal. Chem., 49 (1977) 564-573.

[20] D. Patra, A.K. Mishra, Recent developments in multi-component synchronous fluorescence scan analysis, Trac-Trends in Analytical Chemistry, 21 (2002) 787-798.

[21] B. Li, P.W. Ryan, M. Shanahan, K.J. Leister, A.G. Ryder, Fluorescence excitation-emission matrix (EEM) spectroscopy for rapid identification and quality evaluation of cell culture media components, Appl. Spectrosc., 65 (2011) 1240-1249.

[22] B. Li, M. Shanahan, A. Calvet, K.J. Leister, A.G. Ryder, Comprehensive, quantitative bioprocess productivity monitoring using fluorescence EEM spectroscopy and chemometrics, Analyst, 139 (2014) 1661-1671.

[23] K. Kumar, A.K. Mishra, Analysis of dilute aqueous multifluorophoric mixtures using excitation-emission matrix fluorescence (EEMF) and total synchronous fluorescence (TSF) spectroscopy: A comparative evaluation, Talanta, 117 (2013) 209-220.

[24] K. Ohadi, R.L. Legge, H.M. Budman, Intrinsic fluorescence-based at situ soft sensor for monitoring monoclonal antibody aggregation, Biotechnol. Progr., 31 (2015) 1423-1432.

[25] R.C. Groza, B. Li, A.G. Ryder, Anisotropy resolved multidimensional emission spectroscopy (ARMES): A new tool for protein analysis, Anal. Chim. Acta, 886 (2015) 133-142.

[26] Y. Casamayou-Boucau, A.G. Ryder, Extended wavelength anisotropy resolved multidimensional emission spectroscopy (ARMES) measurements: better filters, validation standards, and Rayleigh scatter removal methods, Methods Appl Fluoresc, 5 (2017) 037001.

[27] S.D. Brown, L.A. Sarabia, J. Trygg, Comprehensive chemometrics chemical and biochemical data analysis, Amsterdam : Elsevier, Amsterdam, 2009.

[28] J.M. Amigo, F. Marini, Multiway Methods, in: F. Marini (Ed.) Chemometrics in Food Chemistry, Elsevier Science Bv, Amsterdam, 2013, pp. 265-313.

[29] C. Ruckebusch, L. Blanchet, Multivariate curve resolution: A review of advanced and tailored applications and challenges, Anal. Chim. Acta, 765 (2013) 28-36.

[30] H. Abdollahi, R. Tauler, Uniqueness and rotation ambiguities in Multivariate Curve Resolution methods, Chemometrics Intellig. Lab. Syst., 108 (2011) 100-111.

[31] R. Bro, PARAFAC. Tutorial and applications, Chemometrics Intellig. Lab. Syst., 38 (1997) 149-171.

[32] C.M. Andersen, R. Bro, Practical aspects of PARAFAC modeling of fluorescence excitation-emission data, J. Chemom., 17 (2003) 200-215.

[33] K.R. Murphy, C.A. Stedmon, D. Graeber, R. Bro, Fluorescence spectroscopy and multi-way techniques. PARAFAC, Analytical Methods, 5 (2013) 6557-6566.

[34] R.C. Groza, A. Calvet, A.G. Ryder, A fluorescence anisotropy method for measuring protein concentration in complex cell culture media, Anal. Chim. Acta, 821 (2014) 54-61.

[35] Y. Casamayou-Boucau, A.G. Ryder, Accurate anisotropy recovery from fluorophore mixtures using Multivariate Curve Resolution (MCR), Anal. Chim. Acta, 1000 (2018) 132-143.

[36] R.C. Groza, Anisotropy Resolved Multi-dimensional Emission Spectroscopy (ARMES): A new tool for the quantitative and structural analysis of proteins. PhD thesis., School of Chemistry, National University of Ireland Galway, Galway, Ireland, 2016.

[37] M. Ameloot, M. vandeVen, A.U. Acuna, B. Valeur, Fluorescence anisotropy measurements in solution: Methods and reference materials (IUPAC Technical Report), Pure Appl. Chem., 85 (2013) 589-608.

[38] M.R. Eftink, L.A. Selvidge, P.R. Callis, A.A. Rehms, Photophysics of indole-derivatives - experimental resolution of La and Lb transition and comparison with theory, J. Phys. Chem., 94 (1990) 3469-3479.

[39] K. Kumar, A.K. Mishra, Multivariate curve resolution alternating least square (MCR-ALS) analysis on total synchronous fluorescence spectroscopy (TSFS) data sets: Comparing certain ways of arranging TSFS-based three-way array, Chemometrics Intellig. Lab. Syst., 147 (2015) 66-74.

[40] K. Kumar, A.K. Mishra, Parallel factor (PARAFAC) analysis on total synchronous fluorescence spectroscopy (TSFS) data sets in excitation-emission matrix fluorescence (EEMF) layout: Certain practical aspects, Chemometrics Intellig. Lab. Syst., 147 (2015) 121-130.

[41] S. Elcoroaristizabal, A. de Juan, J.A. Garcia, N. Durana, L. Alonso, Comparison of second-order multivariate methods for screening and determination of PAHs by total fluorescence spectroscopy, Chemometrics and Intelligent Laboratory Systems, 132 (2014) 63-74.

[42] M. Bahram, R. Bro, C. Stedmon, A. Afkhami, Handling of Rayleigh and Raman scatter for PARAFAC modeling of fluorescence data using interpolation, J. Chemom., 20 (2006) 99-105.

[43] S. Elcoroaristizabal, R. Bro, J.A. Garcia, L. Alonso, PARAFAC models of fluorescence data with scattering: A comparative study, Chemometrics Intellig. Lab. Syst., 142 (2015) 124-130.

[44] A. Rinnan, K.S. Booksh, R. Bro, First order Rayleigh scatter as a separate component in the decomposition of fluorescence landscapes, Anal. Chim. Acta, 537 (2005) 349-358.

[45] D.N. Kothawala, K.R. Murphy, C.A. Stedmon, G.A. Weyhenmeyer, L.J. Tranvik, Inner filter correction of dissolved organic matter fluorescence, Limnology And Oceanography-Methods, 11 (2013) 616-630.

[46] M. Tarai, A.K. Mishra, Inner filter effect and the onset of concentration dependent red shift of synchronous fluorescence spectra, Anal. Chim. Acta, 940 (2016) 113-119.

[47] R.C. Groza, A. Calvet, A.G. Ryder, A fluorescence anisotropy method for measuring protein concentration in complex cell culture media, Analytica Chimica Acta, 821 (2014) 54-61.

[48] A. Savitzky, M.J.E. Golay, Smoothing + Differentiation of Data by Simplified Least Squares Procedures, Anal. Chem., 36 (1964) 1627-&.

[49] R. Bro, H.A.L. Kiers, A new efficient method for determining the number of components in PARAFAC models, J. Chemom., 17 (2003) 274-286.

[50] R. Boteva, T. Zlateva, V. DorovskaTaran, A. Visser, R. Tsanev, B. Salvato, Dissociation equilibrium of human recombinant interferon gamma, Biochemistry, 35 (1996) 14825-14830.

[51] J. Eisinger, B. Feuer, A.A. Lamola, Intramolecular Singlet Excitation Transfer. Applications to Polypeptides, Biochemistry, 8 (1969) 3908-+.

[52] J. Eisinger, Intramolecular Energy Transfer in Adrenocorticotropin, Biochemistry, 8 (1969) 3902-&.

[53] H.C. Chiu, R. Bersohn, Electronic-Energy Transfer Between Tyrosine and Tryptophan in Peptides Trp-(Pro)N-Tyr, Biopolymers, 16 (1977) 277-288.

[54] A.P. Demchenko, The red-edge effects: 30 years of exploration, Luminescence, 17 (2002) 19-42.

[55] B. Li, A.G. Ryder, Similarity index: a rapid classification method for multivariate data arrays, Google Patents, 2011.

[56] T.J. Kamerzell, J.D. Ramsey, C.R. Middaugh, Immunoglobulin dynamics, conformational fluctuations, and nonlinear elasticity and their effects on stability, Journal of Physical Chemistry B, 112 (2008) 3240-3250.

[57] K. Lim, D.M. Jameson, C.A. Gentry, J.N. Herron, Molecular-dynamics of the antifluorescein-4-4-20 antigen-binding fragment. 2. Time-resolved fluorescence spectroscopy, Biochemistry, 34 (1995) 6975-6984.

[58] D.C. Hanson, J. Yguerabide, V.N. Schumaker, Segmental flexibility of immunoglobulin-G antibody molecules in solution - a new interpretation, Biochemistry, 20 (1981) 6842-6852.

[59] R.C. Groza, B.Y. Li, A.G. Ryder, Anisotropy resolved multidimensional emission spectroscopy (ARMES): A new tool for protein analysis, Anal. Chim. Acta, 886 (2015) 133-142.

[60] L.W. Runnels, S.F. Scarlata, Theory and Applications of Fluorescence Homotransfer to Melittin Oligomerization, Biophys. J., 69 (1995) 1569-1583.

[61] G. Weber, Fluorescence-polarization spectrum and electronic-energy transfer in tyrosine, tryptophan and related compounds, Biochem. J, 75 (1960) 335-345.

[62] G. Weber, Fluorescence-polarization spectrum and electronic-energy transfer in proteins, Biochem. J, 75 (1960) 345-352.

[63] B. Valeur, G. Weber, Resolution of Fluorescence Excitation Spectrum of Indole into 1La and 1Lb Excitation Bands, Photochem. Photobiol., 25 (1977) 441-444.

[64] R.J. Robbins, G.R. Fleming, G.S. Beddard, G.W. Robinson, P.J. Thistlethwaite, G.J. Woolfe, Photophysics of Aqueous Tryptophan - pH and Temperature Effects, J. Am. Chem. Soc., 102 (1980) 6271-6279.

[65] E.A. Burstein, N.S. Vedenkina, M.N. Ivkova, Fluorescence and Location of Tryptophan Residues in Protein Molecules, Photochem. Photobiol., 18 (1973) 263-279.

[66] Y.K. Reshetnyak, E.A. Burstein, Decomposition of protein tryptophan fluorescence spectra into log-normal components. II. The statistical proof of discreteness of tryptophan classes in proteins, Biophys. J., 81 (2001) 1710-1734.